TECHNICAL ARTICLE

Phase composition and microstructure of new Ti–Ta–Nb–Zr biomedical alloys prepared by mechanical alloying method

G. Dercz,[1,a)] I. Matuła,[1] M. Zubko,[1] and J. Dercz[2]
[1]*Institute of Materials Science, University of Silesia, 75 Pułku Piechoty Street 1 A, 41-500 Chorzów, Poland*
[2]*Institute of Technology and Mechatronics, University of Silesia, Śnieżna 2, 41-200 Sosnowiec, Poland*

(Received 16 October 2016; accepted 29 December 2016)

The study presents the results of the influence of high-energy ball-milling time on the structure of the new β-type Ti–Ta–Nb–Zr alloys for biomedical applications. Initial elemental powders were mechanically alloyed in a planetary high-energy ball mill at different milling times (from 10 to 90 h). Observation of the powder morphology after various stages of milling leads to the conclusion that with the increase of the milling time the size of the powder particles as well as the degree of aggregation change. Clear tendency of crystalline size reduction at every stage of the grinding process is clearly observed. The X-ray diffraction results confirmed the formation of β phase during high-energy ball milling of the precursor mixture of Ti, Ta, Nb, and Zr. The Rietveld refinement method has shown that both the production method and the atomic radii of the elements used in the mechanical synthesis have influence on the structure. Furthermore, it was found that a broadening of the diffraction peaks with increase of the milling time results from an increase in the crystallites dispersion and an enlargement in the lattice distortion. The results indicate that this technique is a powerful and high productive process for preparing new β-titanium alloys with nanocrystalline structure and appropriate morphology. © *2017 International Centre for Diffraction Data*. [doi:10.1017/S0885715617000045]

Key words: Rietveld method, nanocrystalline materials, Ti–Ta–Nb–Zr alloys, mechanical synthesis

I. INTRODUCTION

Titanium-based alloys are a very attractive material for biomedical applications, in particular for long-lasting bone implants (Long and Rack, 1998; Brunette *et al.*, 2001). The advantages of this material such as: high biocompatibility, very high resistance to corrosion, ability to self-passivation, low thermal conductivity, and high mechanical strength contribute to the fact that this material is widely used in medicine (Long and Rack, 1998; Brunette *et al.*, 2001; Geetha *et al.*, 2009). In addition, pure Ti and Ti-based alloys have been widely employed in biomedical applications because these alloys have lower density and the lowest Young's modulus in comparison with other metals currently used for medical implants (Geetha *et al.*, 2009). Titanium has allotropy properties; exhibits a hexagonal closely packed (*hcp*) crystalline structure at room temperature, called α phase, that changes to a body centered cubic crystalline structure, called β phase, when temperature exceeds 882 °C (Long and Rack, 1998). Mechanical properties of the α phase and the β phase are different; the α phase exhibits good strength and creep resistance and the β phase exhibits high fatigue resistance and low elastic modulus. These characteristics make Ti-based alloys composed with β phase and non-toxic elements (Nb, Ta, Zr, Mo, and Sn) a good candidate for a biomaterials design. The β phase can be stabilized at room temperature by addition of alloying elements. These elements are non-toxic to human body and can strengthen the Ti-matrix through solid solutions (Long and Rack, 1998; Eisenbarth *et al.*, 2004).

Conventionally, these alloys are prepared by melting techniques, in an arc furnace, followed by specific thermomechanical treatments for homogenization and aging and additional mechanical machining in order to obtain the desired shape (Kim *et al.*, 2005; Cui and Guo, 2009). All these processes are done under vacuum or inert atmosphere because oxidation drastically damages the properties. Recently, there has been significant interest in adopting new non-conventional techniques such as powder metallurgy (PM) (Nouri *et al.*, 2011; Hsu *et al.*, 2014). The PM process is a good way to synthesize Ti-based alloys because it makes possible to obtain net-shaped components and materials with a wide spectrum of properties. An interesting PM-processing technique is mechanical alloying (MA), which makes possible to produce micro and nanocrystalline Ti-based alloys (Nouri *et al.*, 2011; Hsu *et al.*, 2014). Nanocrystalline materials based on titanium alloys have become a subject of both scientific and industrial importance in the past decades because of their novel properties such as elasticity, hardness, crystalline phases, biocompatibility, corrosion resistance, etc. They can be defined as materials comprising single- or multiphase polycrystalline solids with the grain size of a few nanometers, typically <100 nm (Shah *et al.*, 2015). At this size, the substance's physical, chemical, and biological properties are different from what they were at the micrometer and larger scales (Shah *et al.*, 2015). The nanostructured powders or particles with very fine crystalline grains can be synthesized by different techniques (Shah *et al.*, 2015). One of them is MA. MA is a prominent synthetic technique involving solid-state reaction

[a)]Author to whom correspondence should be addressed. Electronic mail: grzegorz.dercz@us.edu.pl

among powders because of high-energy collisions, as proved by Suryanarayana (2001). This offers many advantages, such as reduced grain size, the formation of extended solid solutions, amorphous, and/or nanocrystalline alloys, intermetallics, composites, and the ability to synthesize alloys from elements with different melting points (Gill *et al.*, 2011; Long *et al.*, 2013; Nazari *et al.*, 2015). These characteristic advantages can lead to excellent mechanical properties as well as other unique properties. Nazari *et al.* studied the effect of compressive mechanical properties of Ti10Nb3Mo alloy with respect to the milling time points (Nazari *et al.*, 2015). These results showed that increasing milling time was beneficial for producing particle refinement and a high alloying rate but at the cost of reducing their compressive mechanical properties. Long *et al.* obtained ultrafine-grained (range between 12 and 30 nm) Ti6Al4 V powder using high-energy ball milling (Long *et al.*, 2013). On the other hand, research carried out by Gill *et al.* proved that the production method has influence on corrosion resistance (Gill *et al.*, 2011). This investigation revealed that the resistance to pitting corrosion of Ti–30Ta is influenced by its manufacturing process. The alloy manufactured by PM was more resistant to localized corrosion as compared with that manufactured by arc-melting (Gill *et al.*, 2011). Additional advantage of PM with the MA method on the production of biomaterials is the possibility to produce highly porous materials. The PM production method allows one to use this technique to control the pore size, shape, and distribution, including the creation of hierarchical and functionally graded pore structures. The use of high-energy ball milling leads to, as a result of milling, to obtaining the powder with different arrangement of the grain size. This, in turn, with the use of different pressure of isostatic hot pressing can lead to obtaining the material with different degree of porosity, which can be used as a frame for bone restoration (Gill *et al.*, 2011).

These study presents the results of the influence of high-energy milling on the structure and morphology of the new Ti–30Ta–10Nb–20Zr (wt%) alloy for biomedical applications. This alloy has a new original chemical composition, belonging to complex multi-elementary alloy systems. The alloy composition is based only on no-toxic alloying elements, in order to be used as candidate material for medical applications. The alloy composition is designed to assure local and systemic biocompatibility features (Ti, Ta, Nb, and Zr are elements with high passivation rate and low ions release) and appropriate mechanical properties (strength and low elastic modulus) by structural manipulations.

II. EXPERIMENTAL DETAILS

A. Specimen preparation

Commercial powders such as Ti [Atlantic Equipment Engineers (AEE), 99.7%, <45 μm], Ta (Sigma Aldrich, 99.9%, <5 μm), Nb [Atlantic Equipment Engineers (AEE), 99.8%, <5 μm] and Zr [Atlantic Equipment Engineers (AEE), purity 99.5%, <300 μm] were used as an initial powder for the synthesis of the alloy. Equilibrium weighted amounts corresponding to the Ti–30Ta–10Nb–20Zr (wt%) were prepared. They underwent high-energy planetary-ball milling in the Fritch Pulverisette 7 premium line mill. The containers and balls that were used were made of hardened steel. The process parameters were as follows: milling speed was 250 rpm and the weight ratio of the balls to the material was 10:1. The milling time was a variable technological parameter and was 10, 20, 30, 50, 60, and 90 h for the respective samples, and the powder was filled up afresh each time. To prevent the powder from oxidation to the minimum, the process was carried out in the argon protective-gas atmosphere. The powders were handled in a glove box chamber under argon gas.

B. Standard

The NIST SRM660a (LaB_6 powder) was used as line profile standard for instrumental broadening determination. The accuracy in unit-cell parameters determination found using alumina plate SRM 1976 standard is ±0.02%.

C. Data collection

The crystal structure and phase content of the obtained milled powders were studied by X-ray diffraction (XRD) with the use of an X-ray X'Pert diffractometer manufactured by Phillips, with the use of a lamp with a copper anode (Cu$K\alpha$ – $\lambda = 1.54178$ Å), powered by the electric current of 30 mA and the voltage of 40 kV, and a curved graphite monochromator for the wavelength coming from the copper anode. The powder pattern was recorded by "step-scanning" of 0.04°2θ step within the angle range from 10 to 140°2θ.

Verification tests of the crystallites were conducted using the electron transmission microscope JEM 3010 operating at the accelerating voltage of 300 kV. The morphology of the samples was tested using the scanning microscope JEOL JSM 6480 with the accelerating voltage of 20 kV. Chemical analysis was performed using the EDS detector manufactured by IXRF using the traditional/standard calibration method.

D. Data reduction

The profile parameters of individual diffraction lines were determined using Toraya PRO-FIT procedure (Toraya, 1996), which applies Pearson VII function for the description of line profiles. The Rietveld analysis was performed applying DBWS-9807 program that is an update version of the DBWS programs for the Rietveld refinement with PC and mainframe computers (Wiles and Young, 1981). The pseudo-Voigt function appeared to be the most useful in describing the diffraction line profiles at Rietveld refinement. The R_{wp} (weighted-pattern factor) and S (goodness-of-fit) parameters were used as numerical criteria of the quality of the fit of calculated to experimental diffraction data (Rietveld, 1969; Young, 1993). The quantitative phase analysis was performed using the relation proposed by Hill and Howard (Hill and Howard, 1987). The XRD lines are broadened mainly because of: (a) instrumental effect, (b) small crystallite size, and (c) lattice distortion. The crystallite sizes of the α and β phases were estimated using Williamson–Hall method (Williamson and Hall, 1953). The size of the crystallites and the lattice distortion were measured by the Williamson–Hall's method .

III. RESULTS AND DISCUSSION

The scanning electron microscopy (SEM) micrographs of the initial metal powders are presented in Figure 1. The

https://doi.org/10.1017/S0885715617000045 Published online by Cambridge University Press

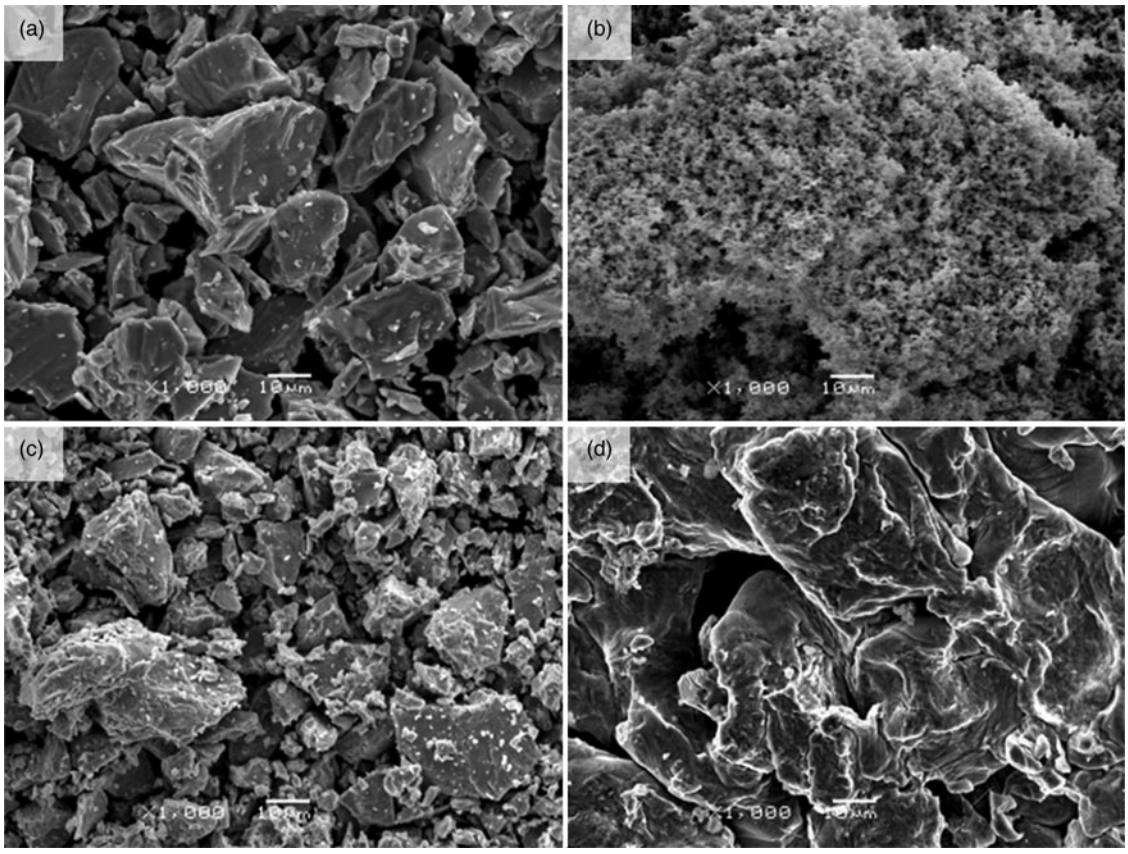

Figure 1. SEM micrographs of initial powders: Ti (a), Ta (b), Nb (c), and Zr (d).

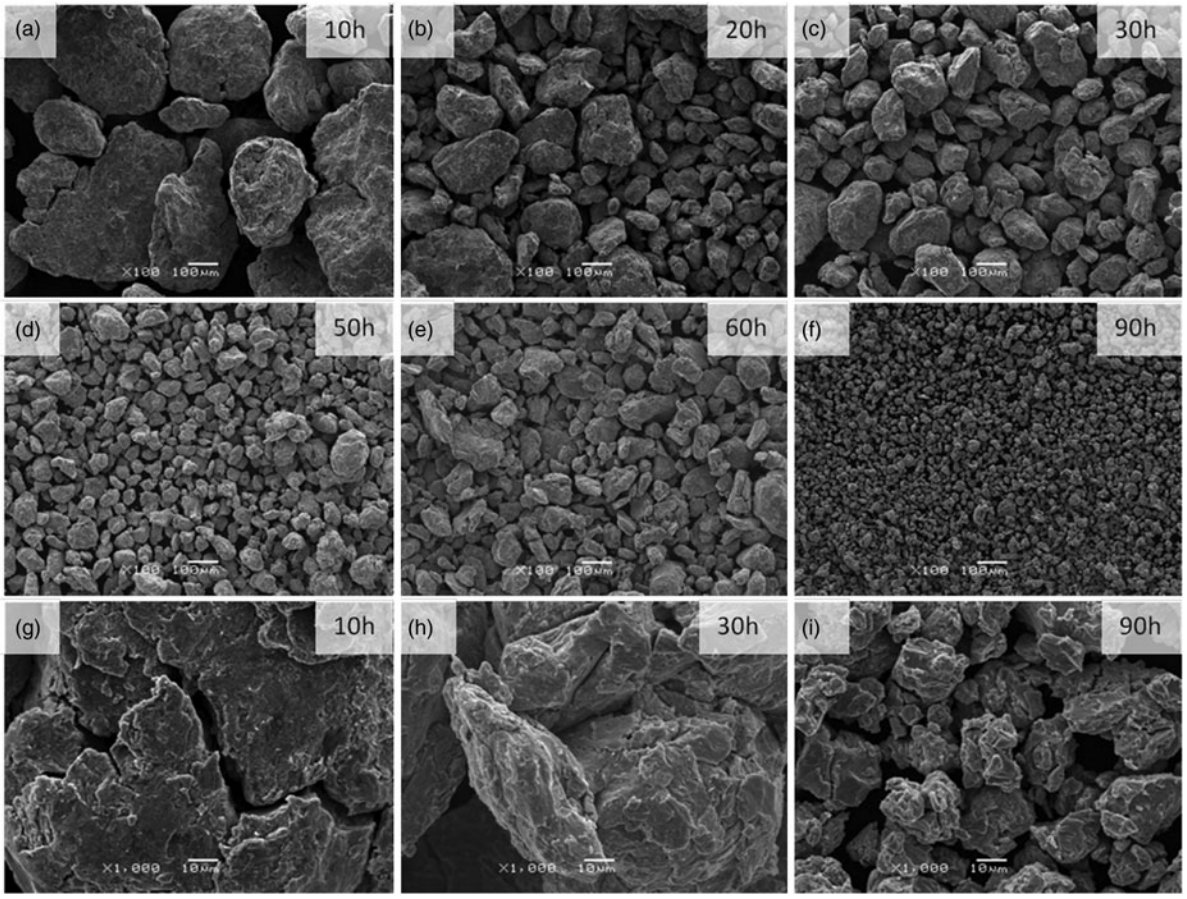

Figure 2. SEM images of powders after: 10 (a, g), 20 (b), 30 (c, h), 50 (d), 60 (e), and 90 (f, i) hours of the milling process.

https://doi.org/10.1017/S0885715617000045 Published online by Cambridge University Press

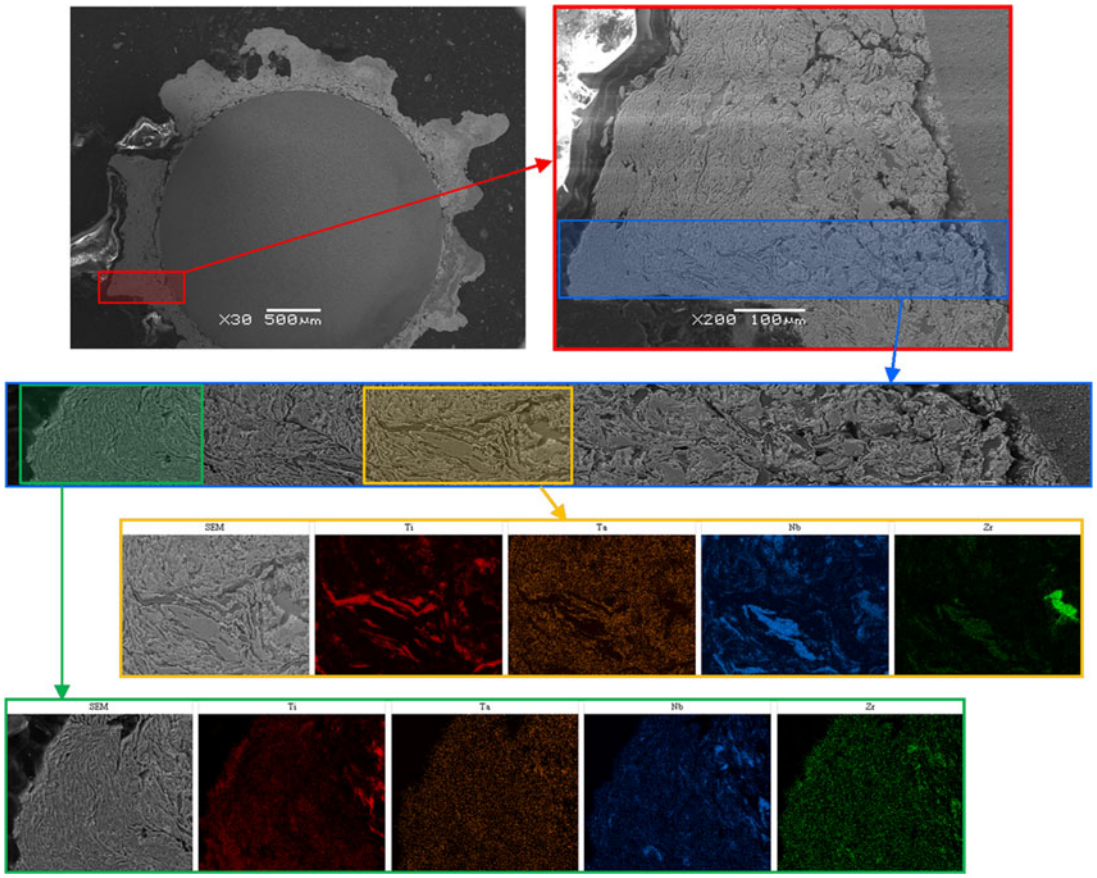

Figure 3. (Colour online) The cross-section of the milling product obtained during the 20-h milling process with distribution of Ti, Ta, Nb, and Zr elements observed on the ball surface.

titanium powder [Figure 1(a)] morphology is irregular with sharp corners. Most particles have the size approximately of 40 μm. In contrast, Ta powders are shattered and joined into agglomerates [Figure 1(b)]. Niobium initial powders had irregular shape of particles, similar to Ti powder. However, the dispersion is much wider in comparison with the titanium powder [Figure 1(c)]. Zirconium powder has the largest particles, which are joined into agglomerates. The shape of particles is irregular but more globular as compared with other initial powders [Figure 1(d)].

Morphology of Ti–30Ta–10Nb–20Zr powders after various milling stages are presented in Figure 2. The microphotographs clearly show progressive changes in the morphology of the particles at different milling stages. It can be seen that at all milling times, the changes of powder particles include two stages. At the first stage, gradual coarsening of powder particles is observed, and the particles evolve from the elemental powder with different morphologies [Figure 2(a)–2(c)] to polygonal particles. At the second stage, particle size decreases progressively, and eventually uniform and finer powder is obtained [Figure 2(f)]. Evidently, intense plastic deformation and cold welding are pronounced in the first stage, while work hardening and fracture play a dominant role at the second stage. During milling in a ball mill for 10 h, a significant advantage of cold welding can be observed [Figure 2(a) and 2(g)]. Further milling results in the formation

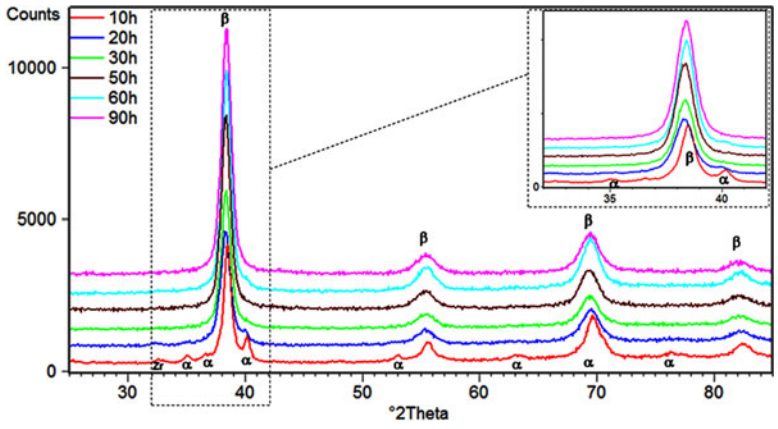

Figure 4. (Colour online) XRD patterns of powder after 10, 20, 30, 50, 60, and 90 h of the milling process.

https://doi.org/10.1017/S0885715617000045 Published online by Cambridge University Press

TABLE I. Changes of the average crystallite size (D) and lattice distortion ($\langle \Delta a/a \rangle$) of α and β phases of the milled samples.

			Milling time (h)					
Phase	Parameters		10	20	30	50	60	90
α	D	(nm)	>100	71(4)	–	–	–	–
	$\langle \Delta a/a \rangle$	(%)	–	0.26(3)	–	–	–	–
β	D	(nm)	>100	48(5)	18(3)	15(2)	15(2)	14(2)
	$\langle \Delta a/a \rangle$	(%)	–	0.28(3)	0.36(3)	0.45(4)	0.50(4)	0.66(5)

TABLE II. Changes of the weight fraction of the α, β, and Zr phases of the milled samples.

		Milling time (h)					
Phase	Weight fraction	10	20	30	50	60	90
α	(%)	19.4(3)	4.2(3)	–	–	–	–
β	(%)	79.5(8)	95.8(8)	100.0	100.0	100.0	100.0
Zr	(%)	1.1(3)	–	–	–	–	–

TABLE III. Unit-cell parameters of α and β phases of the milled powder.

			Milling time (h)					
Phase	Unit-cell parameters	ICDD	10	20	30	50	60	90
α	a_0 (nm)	0.2970	0.2962(3)	0.2953(3)	–	–	–	
	c_0 (nm)	0.4720	0.4651(4)	0.4679(3)	–	–	–	–
β	a_0 (nm)	0.3307	0.3305(4)	0.3307(4)	0.3315(3)	0.3315(4)	0.3314(3)	0.3314(4)

*International Centre for Diffraction Data®.

of agglomerates. Microphotographs [Figure 2(b), 2(c), and 2 (h)] of the powders milled in a ball mill for 20 and 30 h showed the appearance of fine particles and many larger agglomerates. The formation of the agglomerated particles is because of the domination of cold welding over fracturing. The structure of the samples shows a breakdown of the grain into smaller particles [Figure 2(d)]. The formation of fine particles and smaller variation in the composition between the particles for longer milling times results in a higher degree of homogeneity. At the stage of milling for 60 [Figure 2(e)] plastic powders are agglomerated into larger particles and further deformation of the charge can be observed. The particles showed irregular sizes – fragmented grains and larger agglomerates could be observed. For the longest milling time another fragmentation of the powder can be observed, which finally leads to obtaining the homogeneous fine-grained (about 10–20 μm) morphology [Figure 2(f) and (i)].

TABLE IV. Values of various reliability parameters as obtained from the Rietveld analysis of the milled powder.

	Milling time (h)					
Refinement parameters	10	20	30	50	60	90
R_{wp} (%)	9.17	10.23	10.93	11.06	10.75	12.51
R_{exp} (%)	4.85	5.14	5.97	5.73	5.51	5.51
S	1.89	1.99	1.83	1.93	1.95	1.95

SEM images of the cross-section of the ball used for 20 h of milling with the cold-welded material (Figure 3) revealed further stages and processes, which occur during the successive cold welding of the material onto the balls. The distribution map of the elements confirmed layered welding of the material enriched in one of the primary elements (yellow frame). It was concluded that an increase of the milling time causes greater fragmentation of the powder and a decrease of the concentration areas of one element at the same time. Observations of the microsection (green frame) revealed that at the end of 20 h of mechanical milling, mechanical synthesis of the primary elements appears.

Figure 4 shows the XRD patterns of the material after MA, depending on the milling time of initial powders. The change of the lines profile on individual diffraction patterns is clearly visible. All XRD patterns revealed existence of the β phase. For the sample milled for 10 h, diffraction lines from Zr were also observed. A higher magnification of the area outlined in Figure 4 is shown, which demonstrates that α phases peaks decrease gradually during MA from 10 to 20 h. After 20 h of milling, the peaks are barely identified. Generally, the disappearance of initial powders peaks is interpreted as the dissolution of minor components in Ti, accompanied by the formation of the β-titanium solid solution. In addition, progressive broadening of diffraction lines is revealed in the XRD patterns as milling time increases, which is because of the decreased grain sizes and accumulation of the lattice strains of the particles and reduction of the size of the crystallites.

https://doi.org/10.1017/S0885715617000045 Published online by Cambridge University Press

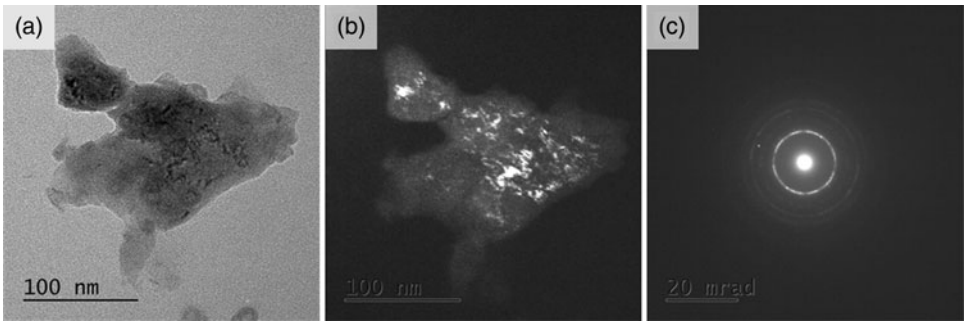

Figure 5. TEM analysis of the powder milled for 60 h; (a, b) are the TEM bright and dark field images, respectively; (c) the corresponding SAED pattern of the β phase.

The Williamson–Hall's method used to analyze the size of the crystallites showed the tendency to decrease the size of the crystallites (D) and increase the lattice distortion ($\langle \Delta a/a \rangle$) typical of the milled materials. It was found that during the 10–20 h of milling the process of nanocrystallization of the powder takes place (Table I). After 30 h of milling the biggest increase of the estimated values of the crystallites for the β phase to the value below 20 nm was registered. Probably it is the result of the disappearance of α phase as well as of the course of MA. Further milling does not reduce the size of the crystallites significantly. However, a continuous increase of the lattice distortion can be observed, which finally reaches 0.66(5) % for the β phase (Table I). It must be stressed that the size of the crystallites does not change despite the fact that an increase of the milling time involves the changes of the grain morphology and size (Figure 2).

The contents of these phases determined using by the Hill and Howard procedure are both presented in Table II.

Table III presents the values of unit-cell parameters determined by using the Rietveld method for all the phases concerned. The unit-cell parameters were calculated from the peak position (2θ) for all the observable reflections using the least-squares method.

Rietveld refinements were performed in order to investigate the influence the addition of Ta, Nb, and Zr on the unit-cell parameters (Table III). In the case of the α phase, while the milling time is increased, a decrease of a_0 parameters is observed along with a simultaneous increase of c_0. The determined c/a ratio increases from 1.5700 to 1.5846, which seems to be the result of the atoms of one of the additions with a higher atomic radius Zr (~0.160 nm) in relation to Ti (~0.147 nm) in the *hcp* spaces. In the case of the β phase for the milling times of 10–50 h, an initial increase of the a_0 parameter was observed, reaching the maximum [0.3315(3) nm] for 30 and 50 h of milling. Owing to the bigger atomic radius of Zr (~0.160 nm) and a similar atomic radius of Ta (~1.46 Å) and Nb (~1.46 Å) compared with Ti (~1.47 Å), the addition of Zr atoms caused the unit-cell parameters of the β phase to expand, which in turn caused the XRD peaks to shift toward the low angle side. Then, gradual decrease of the size of the unit cell takes place in order to finally reach the value of $a_0 = 0.3314(4)$. Contraction of the unit cell of the β phase after MA is the result of strong mechanical effects during the longest milling times.

During the Rietveld analysis, the R_{wp} convergence coefficient values were between 9.1 and 12.51% for all the milled powders, and the S convergence quality coefficient values were between 1.89 and 1.99. They are presented in Table IV together with the R_{exp} coefficient. These values must be regarded as very good, taking into account the fact that the materials that were analyzed contained the nanometric phases.

The effect of the long-term high-energy milling on the structure of the powder after 60 h of milling confirmed its nanocrystallite character using a transmission electron microscope (TEM). The analysis of the obtained images recorded in bright and dark field and of the diffraction image proved the nanocrystalline nature of the material after milling (Figure 5). Sample images of the powder after 60 h of milling obtained in the bright and dark field show that a single particle of the powder is composed of many smaller crystallites with different orientations (Figure 5). Analysis of the selected area electron diffraction (SAED) pattern confirmed that obtained material possesses β phase structure.

VI. CONCLUSION

(1) The XRD analysis showed the complete transformation of the produced new Ti–30Ta–10Nb–20Zr alloy from the α-Ti phase to the β-Ti phase after 30 h of milling using high-energy ball milling.
(2) Based on the cross-section analysis of the material from the ball surface, it was found that the synthesis of the initial components begins before 20 h of milling.
(3) The effect of the high-energy milling time of the substrates on the structure and phase composition of the Ti–30Ta–10Nb–20Zr (wt%) alloy was observed. X-ray and electron microscopy studies confirmed the presence of α- and β-nanocrystalline phases.
(4) During MA, Ti–30Ta–10Nb–20Zr powder particles coarsen at the first stage because of plastic deformation and cold welding, and then refine gradually because of work hardening and fracture.

ACKNOWLEDGEMENT

This work was supported by the Polish National Science Centre (Polish: Narodowe Centrum Nauki, abbr. NCN) under the research project No. UMO-2011/03/D/ST8/04884.

Brunette, D. M., Tengvall, P., Textor, M., and Thomsen, P. (Eds.) (**2001**). *Titanium in Medicine* (Springer, New York).

Cui, W. F. and Guo, A. H. (**2009**). "Microstructures and properties of biomedical TiNbZrFe titanium alloy under aging conditions," Mater. Sci. Eng. A **32**, 258–262.

https://doi.org/10.1017/S0885715617000045 Published online by Cambridge University Press

Eisenbarth, E., Velten, D., Müller, M., Thull, R., and Breme, J. (**2004**). "Biocompatibility of beta-stabilizing elements of titanium alloys," Biomaterials **25**, 5705–5713.

Geetha, M., Singh, A. K., Asokamani, R., and Gogia, A. K. (**2009**). "Ti based biomaterials, the ultimate choice for orthopaedic implants – a review," Progr. Mater. Sci. **54**, 397–425.

Gill, P., Pandya, S., and Haider, W. (**2011**). "Effect of manufacturing process on the biocompatibility and mechanical properties of Ti–30Ta alloy," J. Mater. Eng. Perform. **20**, 819–823.

Hill, R. J. and Howard, C. J. (**1987**). "Quantitative phase analysis from neutron powder diffraction data using the Rietveld method," J. Appl. Crystallogr. **20**, 467–474.

Hsu, H. C., Wu, S. C., Hsu, S. K., Chang, T. Y., and Ho, W. F. (**2014**). "Effect of ball milling on properties of porous Ti–7.5Mo alloy for biomedical applications," J. Alloys Compd. **582**, 793–801.

Kim, J. I., Kim, H. Y., Inamura, T., Hosoda, H., and Miyazaki, S. (**2005**). "Shape memory characteristics of Ti–22Nb–(2–8)Zr(at.%) biomedical alloys," Mater. Sci. Eng. A **403**, 334–339.

Long, M. and Rack, H. J. (**1998**). "Titanium alloys in total joint replacement—a materials science perspective," Biomaterials **19**(18), 1621–1639.

Long, Y., Zhang, H., Wang, T., Huang, X., Li, Y., Wu, J., and Chen, H. (**2013**). "High-strength Ti–6Al–4 V with ultrafine-grained structure fabricated by high energy ball milling and spark plasma sintering," Mater. Sci. Eng. A **585**, 408–414.

Nazari, K. A., Nouri, A., and Hilditch, T., (**2015**). "Effects of milling time on powder packing characteristics and compressive mechanical properties of sintered Ti–10Nb–3Mo alloy," Mater. Lett. **140**, 55–58.

Nouri, A., Hodgson, P. D., and Wen, C. (**2011**). "Effect of ball-milling time on the structural characteristics of biomedical porous Ti–Sn–Nb alloy," Mater. Sci. Eng. C **31**, 921–928.

Rietveld, H. M. (**1969**). "A profile refinement method for nuclear and magnetic structure," J. Appl. Crystallogr. **3**, 65–69.

Shah, M., Fawcett, D., Sharma, S., Tripathy, K., and Poinern, G. E. (**2015**). "Green synthesis of metallic nanoparticles via biological entities," Materials **8**, 7278–7308.

Suryanarayana, C. (**2001**). "Mechanical alloying and milling," Progr. Mater. Sci. **46**, 1–184.

Toraya, H. (**1996**). "Whole-powder-pattern fitting without reference to a structural model: application to X-ray powder diffraction data," J. Appl. Crystallogr. **19**(6), 440–447.

Wiles, D. B. and Young, R. A. (**1981**). "A new computer program for Rietveld analysis of X-ray powder diffraction patterns," J. Appl. Crystallogr. **14**, 149–151.

Williamson, G. K. and Hall, W. H. (**1953**). "X-ray line broadening from filed aluminum and wolfram," Acta Metall. **1**, 22–31.

Young, R. A. (**1993**). *The Rietveld Method* (Oxford University Press, New York).

https://doi.org/10.1017/S0885715617000045 Published online by Cambridge University Press